



**ARTICLE**

# Optimum Calcination Condition of Waste Stabilized Adobe for Alkali Activated High Volume Adobe-Slag Binder Cured at Room Temperature

Brya Aldawoodi<sup>1,\*</sup>, Salaheddin Sabri<sup>1</sup> and Abdulmounem Alchekh Wis<sup>2</sup>

<sup>1</sup>Department of Civil Engineering, Cyprus International University, Haspolat, North Cyprus, via Mersin 10, Turkey

<sup>2</sup>Kocaeli University, Kocaeli, 41380, Turkey

\*Corresponding Author: Brya Aldawoodi. Email: brya.aziz@gmail.com

Received: 11 May 2021 Accepted: 30 July 2021

## ABSTRACT

This study aims to determine the most convenient calcination temperature and calcination duration of waste-stabilized Adobe (AB) to produce a new alkali-activated binder. Waste-stabilized Adobe mainly consists of soil,  $\text{CaCO}_3$  as a stabilizer, and straw (for strengthening). The availability of raw materials for making Adobe presents the waste-stabilized Adobe as a potential product for a new alkali-activated binder. Waste-stabilized Adobe collected from an abandoned damaged building in the village of Inonu in Northern Cyprus, ground and calcined at the following temperatures: 450, 550, 650, 750, 850, and 950°C. The calcination at each temperature was held for different durations 1, 3, 5, and 7 h. Raw and calcined waste stabilized Adobe structures were investigated using XRF, TGA-DTA, XRD, FTIR, and SEM. Considering technical and environmental views related to energy consumption, waste stabilized Adobe calcined at 750°C for 1 h presented the most promising results regarding the production of a new precursor for alkali-activated binder. This study also presents the effect of ground granulated blast furnace slag (GGBFS) usage on the fresh and hardened properties of optimum calcined AB-based alkali-activated pastes cured at room temperature. GGBFS was used to partially replace AB to form a binary composite raw material system and seven experimental groups were designed according to replacement levels of 0%, 5%, 10%, 15%, 20%, 25% and 30% (by mass). Alkali-activated high volume waste-stabilized Adobe-slag pastes prepared using  $\text{Na}_2\text{SiO}_3$ -to- $\text{NaOH}$  ratio of 2 and 12 M concentration of Sodium Hydroxide. The fresh property as flowability and the hardened property as the compressive strength of the alkali-activated pastes with different GGBFS contents were investigated. The results indicated that the incorporation of GGBFS increased the flowability of fresh alkali-activated pastes. A 28-day compressive strength of 43.75 MPa can be obtained by a 30% replacement level of GGBFS.

## KEYWORDS

Waste stabilized adobe; calcination; alkali activation; compressive strength; room temperature curing

## 1 Introduction

Alkali activation for producing new construction materials has been the focus of extensive research in recent years, due to the potential of lower energy and carbon costs compared to traditional materials such as Portland cement-based concrete [1]. Alkali-activated material is the most comprehensive classification, which comprises any binder system obtained from the reaction of an alkaline salt (solid or dissolved)



with a solid silicate powder [2]. Alkali-activation can be classified based on the prime materials utilized by using two models. The first model involves the activation of blast furnace slag (Si + Ca) with a mild alkaline solution, having calcium silicate hydrate (C-S-H) as the major product of reaction [3]. When using the second model of alkali activation (Si + Al), the most popular case is the alkali-activation of metakaolin with moderate to high alkaline solutions. A three-dimensional gel represents the main reaction product for the second model of alkali activation [4].

The progress and evaluation of alkali-activated binders by using calcium-rich precursors, for example, blast furnace slag with other Ca-rich industrial waste-products have been utilized for more than 100 years. Alkali-activation of blast-furnace slag has been used as an alternative means of cement production for over 65 years [5]. Together with industrial by-products like fly ash [6,7] and rice husk ash [8], alkali activation of clays and soils have been studied, because they are cheap and available in abundance [9,10]. Clays may be used as supplementary cementitious materials [11–14], and also as major aluminosilicate (Si + Al) precursors in alkali activation. While little research has been carried out on montmorillonitic and illitic soils, studies of clay minerals in isolation have been overshadowed by kaolinite and metakaolin [15]. Calcined clay soil has been studied by many researchers as a binder for the alkali activation process [16].

Adobe and related materials are considered one of the earliest building materials used by man, with rammed earth construction dating to the Neolithic period (10,000 to 3,000 B.C.) [17]. Until recent decades, Adobe was widely used as a construction material in Northern Cyprus due to the availability of its raw materials and many technical benefits [18]. Adobe can be prepared by mixing soil with water to a plastic consistency, which can be cast into the desired shape, used as mortar between stone or adobe brick, or used as plaster. In many instances, straw was added to adobe to reduce the possibility of cracking [19]. Stabilized adobe contains a stabilizing element that is added to improve the scant moisture resistance of traditional adobe [20]. Gypsum or limestone can be used as a stabilizer for Adobe according to the availability of these materials in the region. Advances in urbanization and extensive use of reinforced concrete materials leave behind many damaged and abandoned buildings constructed from stabilized adobe products scattered in various places in Northern Cyprus. These abandoned buildings are considered as a source of waste stabilized adobe which needs to be evaluated as a resource.

As stabilized Adobe contains Si coming from soil and straw, Ca coming from stabilizer source (Gypsum or limestone), the calcined stabilized Adobe may be considered as a potential source that meets the criteria of the first type of alkali-activated binders (Si + Ca). However, the effects of calcination conditions (temperature and duration) need to be investigated by using several techniques (XRF, DTA/TGA, XRD, FTIR, and SEM) to find an optimum calcination temperature and duration. The binding value (measured by compressive strength at different ages at room temperature curing) of the optimum calcined waste stabilized Adobe as a new precursor (with/out alkali activation) will also be investigated.

The incorporation of an external source of calcium to enhance the fresh and hardened properties of alkali-activated binder in an attempt to minimize the utilization of post-manufacture heat treatment was confirmed by research done by [21] and [22], in their studies, OPC in different percentages are used as an external source of Ca enhancing the properties of activated Class C Fly Ash. It was discovered that the incorporation of OPC enhanced the setting properties in addition to the early strength of the OPC-fly ash alkali-activated system. According to recent studies, Ground Granulated Blast Furnace Slag (GGBFS) and High Calcium Fly Ash are generally used in alkali-activated systems to enable essential hardening of the binder matrix [23–28]. The results of all the reviewed studies came to the same conclusion. The setting, mechanical, and durability properties of the forming binder were made better as a result of presenting calcium ions in the alkali-activated system.

Preparing alkali-activated binder from optimum calcined waste stabilized Adobe as the main precursor and a waste rich in calcium not only extends the source of raw materials for solid waste based alkali-activated

binder, but also solves the problem of space occupied by waste and pollution yielding better environmental outcomes. The process of activation of the optimum calcined waste-stabilized Adobe without incorporation of any external source of calcium may not develop a good strength especially during the early days of curing at room temperature. Therefore, GGBFS was selected as a partial replacement of optimum calcined waste-stabilized Adobe at different proportions to improve both fresh and hardened properties.

The aim of this study is to investigate the effects of calcination conditions on the assessment of waste-stabilized Adobe as a new alkali-activated binder source and the effect of incorporating ground granulated blast furnace slag to enhance its properties. The production of alkali-activated binders (AAB) based on a combination of optimum calcined waste-stabilized Adobe and GGBFS provides an opportunity to overcome some of the difficulties that are possible in AAB formulation, which can include for example, the requirement of high-temperature curing, inadequate workability, or slow strength development.

## 2 Materials and Methods

### 2.1 Materials

#### 2.1.1 Waste Stabilized Adobe Samples

The adobe samples were collected as waste from a demolished and abandoned building in Inonu village in Northern Cyprus. Adobe samples were dried at 105°C for 24 h to remove any moisture. Then the samples were ground using a Los Angeles machine to powder form. Finally, the resulting powder was sieved using a 75 µm sieve. The main oxides content in raw waste-stabilized Adobe are CaO (29.44%), SiO<sub>2</sub> (32.82%), Al<sub>2</sub>O<sub>3</sub> (7.505%), MgO (4.006%) and Fe<sub>2</sub>O<sub>3</sub> (5.705%). The fineness of raw waste stabilized Adobe is (5914 cm<sup>2</sup>/g) found by Blaine fineness method.

#### 2.1.2 Calcination Process

Before the calcination process, adobe waste was kept at 105°C for 24 h to ensure complete drying. The powdered adobe was calcined at different temperatures 450, 550, 650, 750, 850, and 950°C and exposure times 1, 3, 5, and 7 h for each temperature. The calcination process was held in an electrical muffle furnace (PLF 110/8) with a heating rate of 10 °C/min. Aiming to obtain a uniform calcining, the electrical muffle furnace has been fed with 200 g of waste adobe (4 ceramic crucibles with 50 g each). Cooling was done slowly by letting the samples stay in the furnace until the inside temperature dropped to room temperature. After the cooling is completed the calcined waste-stabilized Adobe powder was sieved using a 75 µm sieve. The fineness of the powdered waste-stabilized Adobe before and after calcination was found by the Blaine fineness method according to ASTM C 204–18 [29].

#### 2.1.3 Ground Granulated Blast Furnace Slag (GGBFS)

A common waste product from steel production is slag which is more widely known as ground granulated blast furnace slag (GGBFS). The main oxides that make up the slag mixture are CaO (38.74%), SiO<sub>2</sub> (39.39%), Al<sub>2</sub>O<sub>3</sub> (11.35%), and MgO (6.90%). The specific gravity of slag is 2.87. The fineness of slag is 3092 cm<sup>2</sup>/g found by the Blaine fineness method.

#### 2.1.4 Alkaline Activator

A combination of two alkaline activators (sodium silicate and sodium hydroxide) were used for the process of activation. The sodium hydroxide is in pellet form with a purity of 96.0% and the sodium silicate is in liquid form. The initial modulus of sodium silicate solution (M ratios of SiO<sub>2</sub>/Na<sub>2</sub>O) used in this research is 2. The sodium hydroxide solution was prepared with a 12 M concentration for all mixes. The two alkaline solutions were mixed 24 h before the time of starting the mixing procedures for all mixes.

## 2.2 Methods

### 2.2.1 XRF and XRD

XRF analyses were performed under laboratory conditions using a Hitachi X-MET8000 Expert Geo instrument. It is equipped with an Rh target X-ray tube of 4 W, 50 kV maximum, and a silicon drift detector.

X-ray diffraction analysis was performed with a Shimadzu XRD-6000 X-ray diffractometer using Cu K $\alpha$  radiation ( $\lambda = 0.154$  nm). The operating conditions were 30 mA and 40 kV at 2°/min in 20–70° scanning range.

### 2.2.2 Thermal Gravimetric Analysis (TGA)

Thermal gravimetric analysis (TGA) was used to determine the thermal stability of the waste-stabilized Adobe under a nitrogen atmosphere. A TA Q50 model TGA (Mettler) instrument was used. Test samples were heated from 100°C to 1000°C temperature at a heating rate of 10 °C/min. A 32-ml/min nitrogen flux was used in the heating chamber to avoid carbonation of the samples during the experiment.

### 2.2.3 Fourier Transform Infrared Spectroscopy (FTIR)

The infrared spectra (FTIR) were obtained at room temperature using the Perkin Elmer spectrum 100 FTIR instrument equipped with a diamond ATR crystal. The samples were analyzed in the range of 4000–600 cm<sup>-1</sup>.

### 2.2.4 Scanning Electron Microscopy (SEM)

SEM imaging was used to characterize the morphology of the waste-stabilized Adobe before and after calcination at 750°C for 1, 3, 5, and 7 h. SEM analysis of the waste materials was performed using a JEOL/JSM-6335F-EDS Electron microscopy.

## 3 Mix Design

A ground granulated blast furnace slag (GGBFS) and optimum calcined waste-stabilized Adobe (AB) were mixed in different proportions (AB:GGBFS) of 100AB, 95AB + 5Slag, 90AB + 10Slag, 85AB + 15Slag, 80AB + 20Slag, 75AB + 25Slag, 70AB + 30Slag. The replacement level of AB by GGBFS was limited to 30% in this study to produce a high volume alkali-activated Adobe-slag binder.

Nine different mixes were prepared. The first mix (100ABW) consists of mixing the AB powder with water without the addition of an alkaline activator at (water/powder) mass ratio of 0.4 for 3 min until the desired flow is achieved.

The second mix (100AB) is performed by mixing the AB powder with the alkaline activator (combination of sodium silicate with sodium hydroxide) solution at the activator/powder mass ratio of 0.4 and mixed for 3 min. Na<sub>2</sub>SiO<sub>3</sub>/NaOH ratio and NaOH concentration were made constant at 2 and 12 M for all the mixes. The prescribed proportion of Na<sub>2</sub>SiO<sub>3</sub> and NaOH was homogenized at least 24 h before the mixing process started.

In the third mix (95AB + 5Slag), which consists of 95% AB powder and 5% slag of the total powder weight. The binder, namely AB powder and GGBFS were initially dry mixed for 2 min before the addition of the alkaline activator. After the addition of the liquid part to the powder, the mixing continues for 3 min until homogeneity is achieved.

The fourth (90AB + 10Slag), fifth (85AB + 15Slag), sixth (80AB + 20Slag), seventh (75AB + 25Slag), and eighth (70AB + 30Slag) mixes were prepared following the previously described procedures. The ninth mix (100Slag), prepared by mixing slag powder with an alkaline activator at an activator/powder mass ratio of 0.4 for 4 min to achieve a workable paste.

After finishing the mixing process in the required proportions according to each mix, the slump and flowability tests were conducted according to ASTM WK 63516 [30]. After that the fresh paste was cast into mold  $50\text{ mm} \times 50\text{ mm} \times 50\text{ mm}$  and vibrated for 2 min on an electrical vibrating table. After that, the molds were sealed in plastic bags to inhibit the evaporation of the water, necessary for achieving the activation process. The specimens were then allowed to be set in controlled laboratory conditions (temperature  $24 \pm 2^\circ\text{C}$ ) for 24 h before remolding. The curing continues at room temperature until the testing ages of 3, 7, 14, and 28 days. The detailed mixture proportions of the alkali-activated high volume waste stabilized Adobe-slag pastes are shown in Table 1.

**Table 1:** Mix proportions and value of compressive strength

Mixes	Alkaline activator	Slump (mm)	Flowability (mm)	Compressive strength (Mpa)			
				3 days	7 days	14 days	28 days
100ABW	—————	20	112	2.3	4.2	6.7	8.2
100AB	SS + SH	18	110	4.51	9.61	12.5	14.73
95AB + 5Slag	SS + SH	19	119	3.33	10.21	15	17.2
90AB + 10Slag	SS + SH	23	143	6.78	13.34	17.91	20.8
85AB + 15Slag	SS + SH	25	143	9.53	17.1	21	24.4
80AB + 20Slag	SS + SH	30	148	13.2	19.41	27.95	31
75AB + 25Slag	SS + SH	35	151	16.4	22.53	31.28	36.33
70AB + 30Slag	SS + SH	37	155	19	25.4	37.4	43.75
100Slag	SS + SH	50	187	31.3	47.81	54.9	61.3

Notes: Alkaline liquid/powder ratio = 0.4; Sodium Silicate (SS)/Sodium Hydroxide (SH) ratio = 2; Sodium Hydroxide (SH) of 12 molarity; Room temperature Curing.

## 4 Result and Discussion

### 4.1 XRF

The result of X-ray fluorescence shows  $\text{SiO}_2$ ,  $\text{CaO}$ ,  $\text{Al}_2\text{O}_3$ ,  $\text{Fe}_2\text{O}_3$ , and  $\text{MgO}$  as the main chemical compositions for the raw waste-stabilized Adobe. The high  $\text{SiO}_2$  content is due to the presence of straw in Adobe. The high calcium content is mainly due to  $\text{CaCO}_3$ , which is used as a stabilizer in the making of Adobe brick. Figs. 1–4 show the main chemical oxides at all calcination temperatures used in this study at specific fixed durations of 1, 3, 5, and 7 h, respectively. The raw waste-stabilized Adobe is used as a reference sample for each calcination period sample.

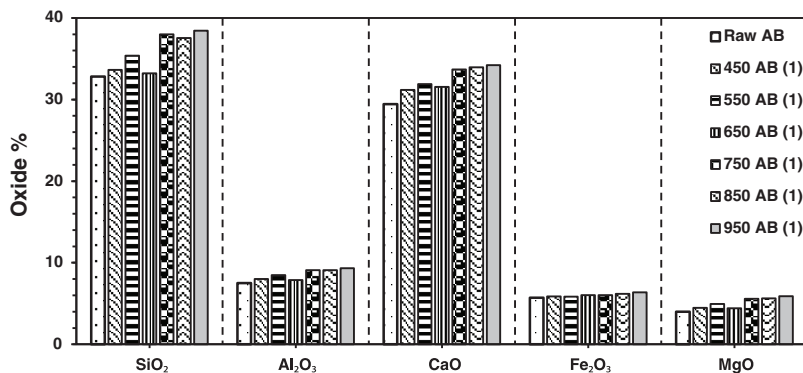


**Figure 1:** Chemical oxides for waste stabilized Adobe for 1 h calcination period

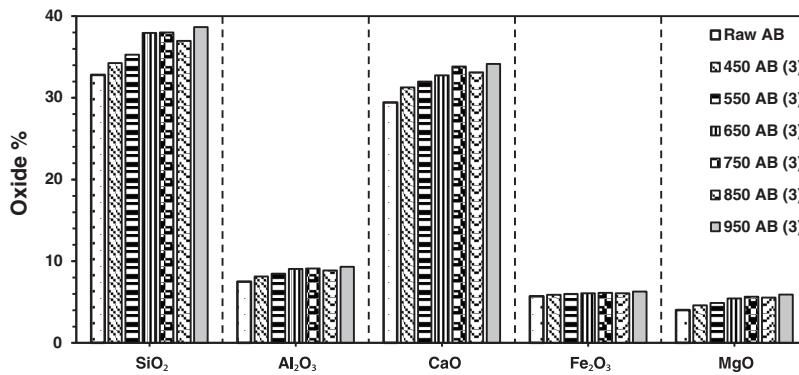


**Figure 2:** Chemical oxides for waste stabilized Adobe for 3 h calcination period

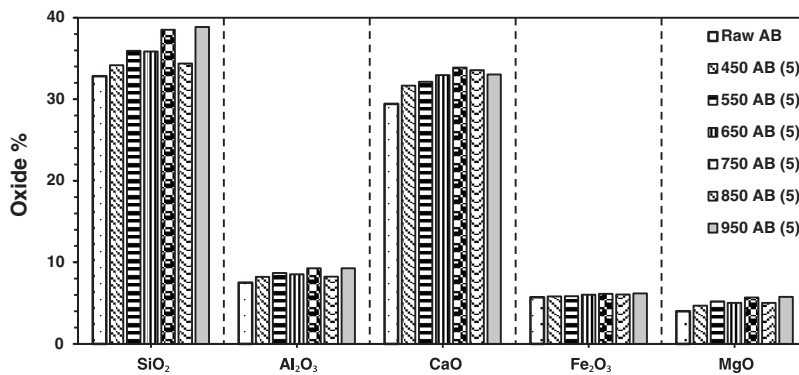


**Figure 3:** Chemical oxides for waste stabilized Adobe for 5 h calcination period

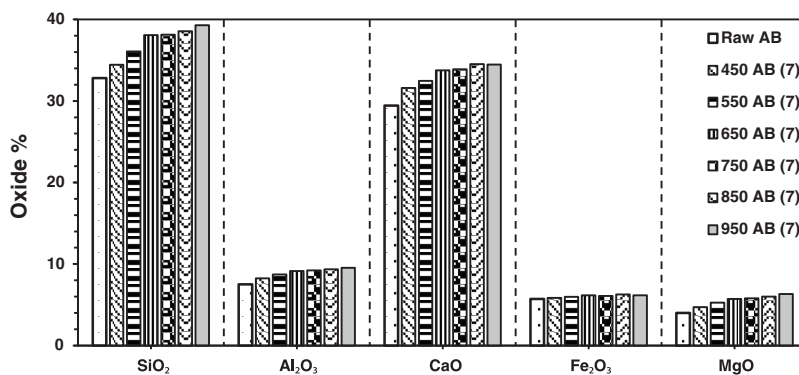


**Figure 4:** Chemical oxides for waste stabilized Adobe for 7 h calcination period

Fig. 1 shows the effect of different calcination temperatures on the main chemical oxides for a calcination period of 1 h. Fe<sub>2</sub>O<sub>3</sub> oxide shows a constant increase with temperature, whereas the other oxides fluctuate as the temperature changes. A drop in all oxides was noticed when the calcination temperature was 650°C with the exception Fe<sub>2</sub>O<sub>3</sub>. There was a small drop in SiO<sub>2</sub> content at 850°C. Generally, SiO<sub>2</sub> and CaO have the highest oxide content at all temperatures.

Fig. 2 shows the effect of different calcination temperatures on the main chemical oxides for waste-stabilized Adobe samples at a calcination period of 3 h. The calcination period has a constant increase for

$\text{Fe}_2\text{O}_3$  whereas it fluctuates in the case of other chemical compositions as shown in Fig. 2. There is a drop in the entire oxide value at the calcination temperature  $850^\circ\text{C}$  for 3 h except for  $\text{Fe}_2\text{O}_3$  which has a constant increase at these calcination periods.

Fig. 3 shows the effect of different calcination temperatures for the same calcination period of five hours, on the main chemical oxides for waste-stabilized Adobe samples. The calcination period (five hours) has an approximate constant increase for  $\text{Fe}_2\text{O}_3$  content whereas it fluctuates in the case of other chemical oxides for all calcination temperatures. There is a drop at  $850^\circ\text{C}$  for the entire chemical oxides at this duration. There is only a drop for the  $\text{Al}_2\text{O}_3$  and  $\text{MgO}$  chemical composition at the temperature of  $650^\circ\text{C}$ .

Fig. 4 shows the effect of different calcination temperatures for the same calcination period (seven hours) on the main chemical oxides for the waste stabilized Adobe samples. This calcination period has an approximate constant increase for  $\text{Al}_2\text{O}_3$  and  $\text{MgO}$  oxides whereas it fluctuates in the case of other chemical oxides. For this calcination duration, there is a drop at  $950^\circ\text{C}$  for the  $\text{CaO}$  and  $\text{Fe}_2\text{O}_3$  oxides. There is a drop for  $\text{Fe}_2\text{O}_3$  oxide at a calcination temperature of  $750^\circ\text{C}$ . At  $650^\circ\text{C}$  there is a drop for the  $\text{Al}_2\text{O}_3$  and  $\text{MgO}$  chemical oxides. Generally,  $\text{SiO}_2$  and  $\text{CaO}$  have the higher oxide content compared to  $\text{Al}_2\text{O}_3$ ,  $\text{Fe}_2\text{O}_3$ , and  $\text{MgO}$  which have the lower oxide content in descending order. The percentage change in oxide content between different temperatures for all calcination periods can be found in Table 1.

#### 4.2 TGA/DTA

The DTA curve for the raw AB is presented in (Fig. 5). The two endothermic peaks present in the raw AB in the temperature range of  $100\text{--}200^\circ\text{C}$  and  $200\text{--}400^\circ\text{C}$  are assigned to the removal of physically adsorbed water [31]. The endothermic peak in the temperature range of  $700\text{--}800^\circ\text{C}$  is attributed to the removal of the OH groups (dehydroxylation) [32]. The decomposition of the raw AB starts at  $700^\circ\text{C}$  and completes between  $750^\circ\text{C}\text{--}773.83^\circ\text{C}$ . The position of the dehydroxylation peak depends mainly on the type of structure and the binding of the hydroxyls, whereas its shape and range depend more on the crystallinity [32]. An exothermic peak was also noticed in the temperature range of  $800\text{--}850^\circ\text{C}$ , and attributed to structural rearrangement of material [33]. The TGA curve is also included in the graph to confirm that the complete dehydroxylation of the raw AB occurred between  $750^\circ\text{C}$  and  $800^\circ\text{C}$ . To get the greatest amorphous phase [14], the temperature selected for calcination must be lower than the temperature of formation of the crystalline phase, and higher than the temperature corresponding to the end of the last endothermic peak. The selected calcined temperature in this study was comparable to the suggestion of [34], which suggests a temperature range of  $650^\circ\text{C}\text{--}800^\circ\text{C}$  for a calcination process.

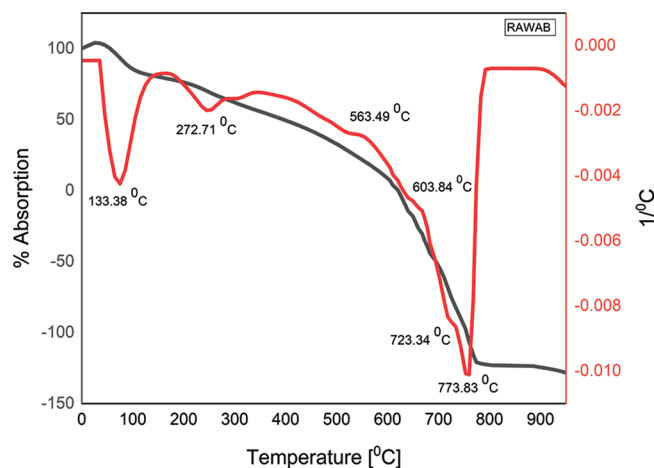
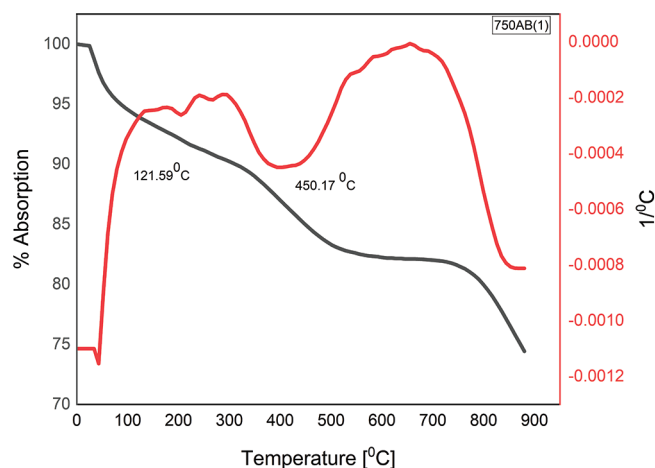
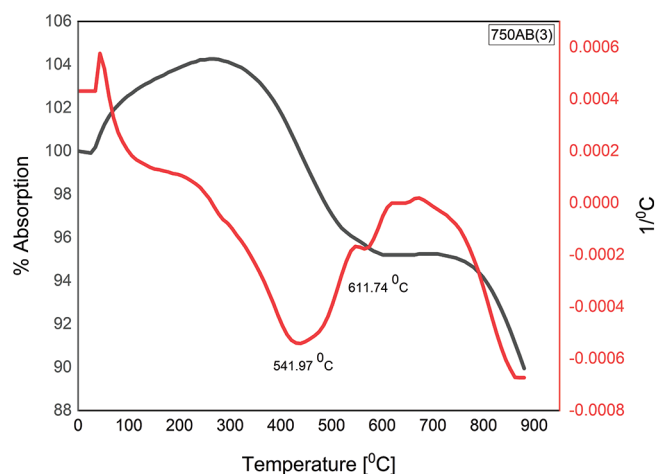


Figure 5: TGA/DTA of raw waste stabilized adobe AB

The DTA curves for the waste-stabilized Adobe calcined at 750°C for different durations 1, 3, 5, and 7 h are presented in Figs. 6–9. The endothermic peaks in the temperature range of 100–200°C and 200–400°C for calcination duration 1 h still appears, while disappearing when prolonging the calcination duration. There is a new endothermic peak in the temperature range of 400–650°C for all durations 1, 3, 5, and 7 h, corresponding to the beginning of decomposition which does not exist in the raw sample. The exothermic peak in the temperature range 600–800°C appears for all calcination duration, which corresponds to complete dehydroxylation, especially at 750°C. Therefore, the calcination duration of 1 h was selected in this study to save more energy in comparison with longer calcination periods 3, 5, and 7 h. This indicates that prolonging the calcination duration for the same calcination temperature did not change the temperature at which complete dehydroxylation occurred.



**Figure 6:** TGA/DTA of 1 h calcined AB at 750°C



**Figure 7:** TGA/DTA of 3 h calcined AB at 750°C

### 4.3 XRD

The XRD patterns for raw waste-stabilized Adobe and calcined waste-stabilized Adobe at 750°C for different durations 1, 3, 5, and 7 h, are shown in Fig. 10. XRD analysis of the raw AB sample showed that quartz and Calcite are the major crystalline components of the sample. Clay minerals (Illite and

kaolinite) were also measured. In general, there is an increase in peak numbers which corresponds to Quartz after calcination at 750°C for all durations. Also, the intensity of some of the peaks increased after calcination at 750°C for all durations as a result of the presence of large amounts of free silica. Diffraction peaks corresponding to Calcite decreased after calcination at 750°C for 1 and 3 h and disappeared when increasing the calcination duration to 5 and 7 h. Diffraction peaks corresponding to Kaolinite and Illite disappeared after calcination at 750°C for 1 h. Prolonging the calcination duration leads to the formation of new phases. Dolomite appears when the sample is calcined at 750°C for 3 h. Akermanite appears when prolonging the calcination duration to between 5 and 7 h. The XRD analysis explained that the calcination of waste stabilized Adobe at 750°C for 1 h is accompanied by the amorphization of most of the phases and reduction of the crystalline percentage. The crystalline percentage in the raw waste-stabilized Adobe is 45.66%. The crystalline percentage after calcination at 750°C for 1, 3, 5 and 7 h are 41.91%, 52.37%, 57.03% and 54.07%, respectively.

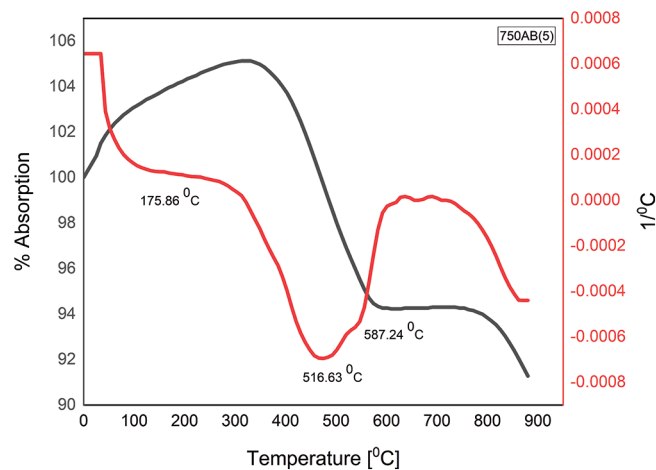


**Figure 8:** TGA/DTA of 5 h calcined AB at 750°C

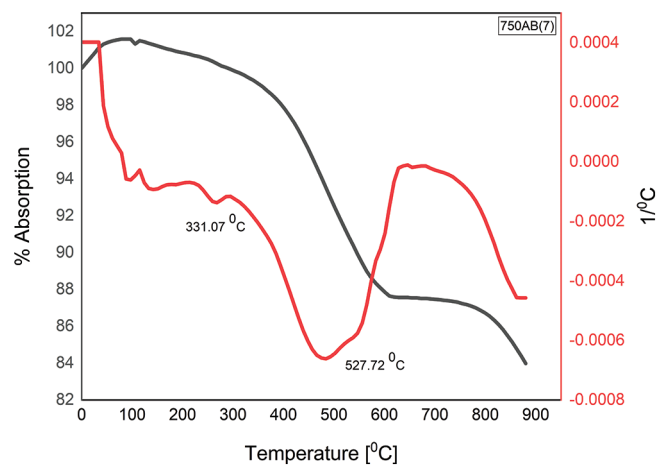


**Figure 9:** TGA/DTA of 7 h calcined AB at 750°C

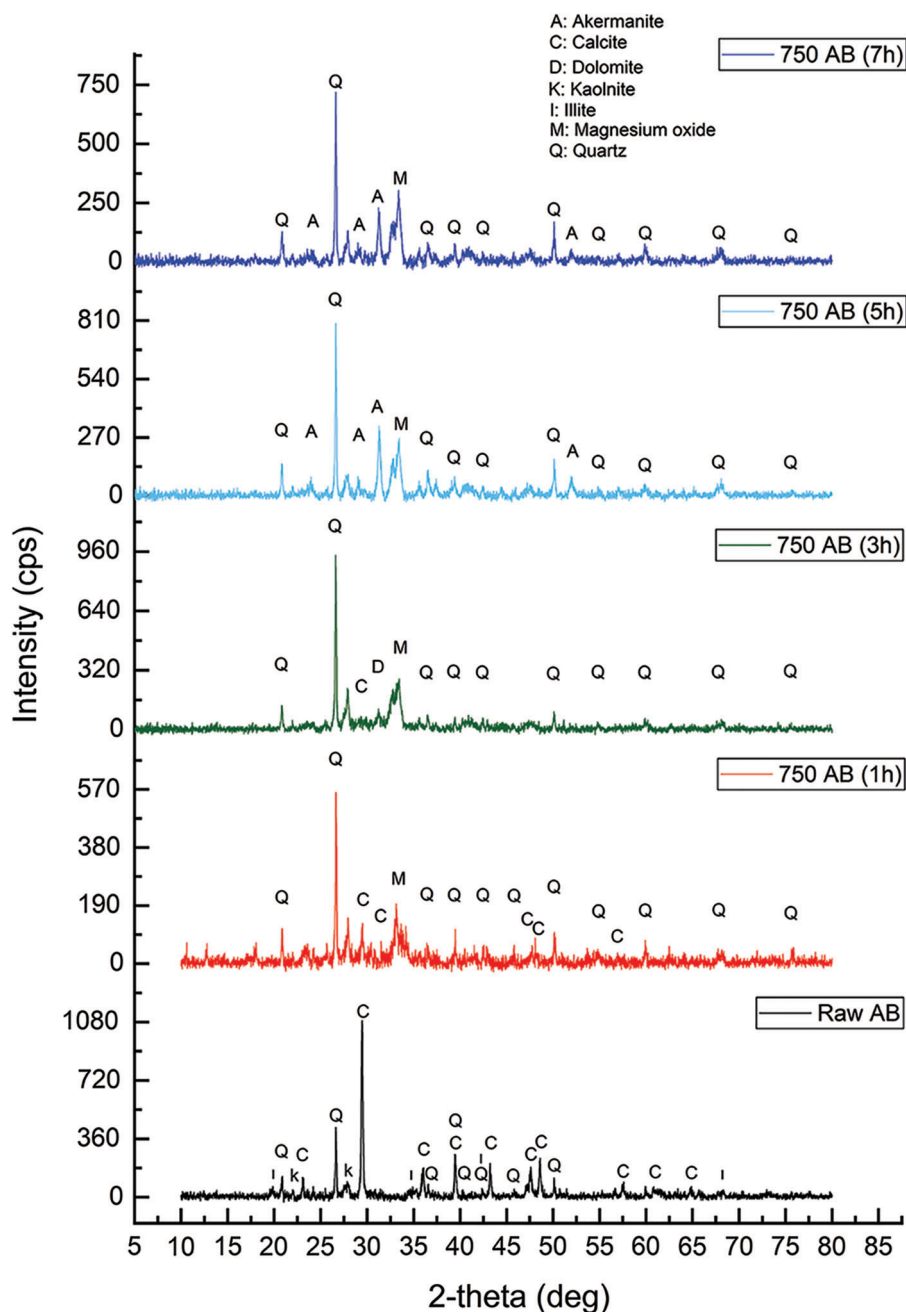


**Figure 10:** Phase composition of Raw and calcined AB at 750°C

#### 4.4 FTIR

The infrared spectra of the raw and calcined AB at 750°C for different duration 1, 3, 5, and 7 h are presented in (Fig. 11). The characteristic band at  $3692.58\text{ cm}^{-1}$  is attributed to the stretching vibration of the hydroxyl groups (OH) of kaolinite and the characteristic band at  $3782.92\text{ cm}^{-1}$  is attributed to the stretching of hydroxyl groups of Illite [35,36]. The band at  $3403.83\text{ cm}^{-1}$  is attributed to the OH stretching of hydrogen-bonded water molecules [37].

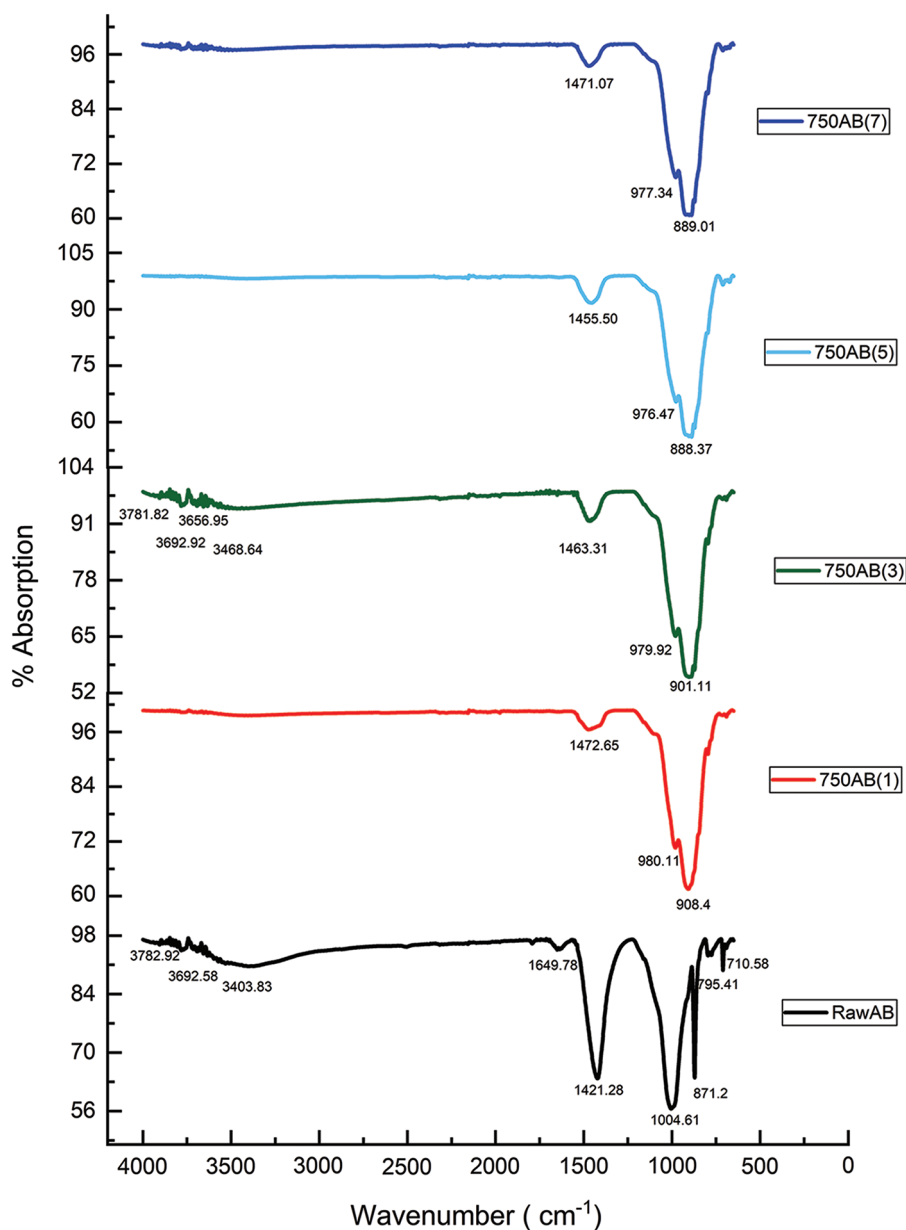


**Figure 11:** FTIR analysis for raw AB and calcined AB at 750°C

The characteristic band at  $1649.78\text{ cm}^{-1}$  refers to the bending vibration of  $\text{H}_2\text{O}$  molecules [38,39], and the band at  $1421.28\text{ cm}^{-1}$  and  $1004.61\text{ cm}^{-1}$  refer to the different elongation mode of Ca-O bonds [40] and Si-O bonds [40], respectively. Calcite ( $\text{CaCO}_3$ ) is observed by the presence of the peak at  $871.2\text{ cm}^{-1}$  [41,42]. The two bands at  $795.41\text{ cm}^{-1}$  and  $710.58\text{ cm}^{-1}$  are assigned to quartz vibrations respectively [43]. This result is in correspondence with that of XRD patterns.

The FTIR results after calcination at  $750^\circ\text{C}$  for different calcination periods 1, 3, 5, 7 h in the spectral range between  $600$  and  $4000\text{ cm}^{-1}$  show the disappearance of O-H bands attributed to kaolinite and those of illite after calcination for 1 h, which indicates that the Kaolinite and Illite structure are disordered and easier to dehydrate [44]. The bands which correspond to kaolinite and illite hydroxyl groups (OH) appear again

after prolonging the calcination time to 3 h because of the process of recrystallization. These bands disappear when prolonging the calcination period to 5 and 7 h. After calcination, there was a disappearance of the band at  $1649.78\text{ cm}^{-1}$  for all calcination periods compared to the raw AB sample. The existence of the band due to the elongation mode of Ca-O bonds can be observed at  $750^\circ\text{C}$  for all four durations.

The shifting of Si-O characteristic bands of kaolinite at  $1004.61\text{ cm}^{-1}$  present in the raw AB to an absorption band at  $980.11\text{ cm}^{-1}$  after calcination, which is characteristic of the amorphous silica. The band at  $908.4\text{ cm}^{-1}$  represents the  $\text{Al}_2\text{OH}$  bending bands of kaolinite. We also note that, after calcination at  $750^\circ\text{C}$ , between  $800$  and  $600\text{ cm}^{-1}$ , the various bands attributed to quartz vibrations disappear, which is following the effects of temperature [44]. Prolonging the calcination duration to 3, 5 and 7 h shows a slight change in the mineral structure of waste-stabilized Adobe.

#### 4.5 SEM

Fig. 12 shows morphological characteristics of raw and calcined waste-stabilized Adobe with a residence time of 1, 3, 5, and 7 h obtained by SEM. The images clearly show a change in surface shape as the exposure to heat increases. Sample of Raw waste-stabilized Adobe presented in Fig. 12a display irregular blocky shaped particles. Fig. 12b shows particles with a rough texture and non-homogeneous size. Figs. 12c and 12e show that prolonging the calcination duration from 3 h to 7 h at  $750^\circ\text{C}$  cause decrease in the small pores that appear on the surface of large particles. It also increases the fine particles attached to the surface of large particles of calcined waste-stabilized Adobe. Fig. 12d shows the flaky morphology of calcined-waste stabilized Adobe at  $750^\circ\text{C}$  for 5 h, stacked in a less dense structure.

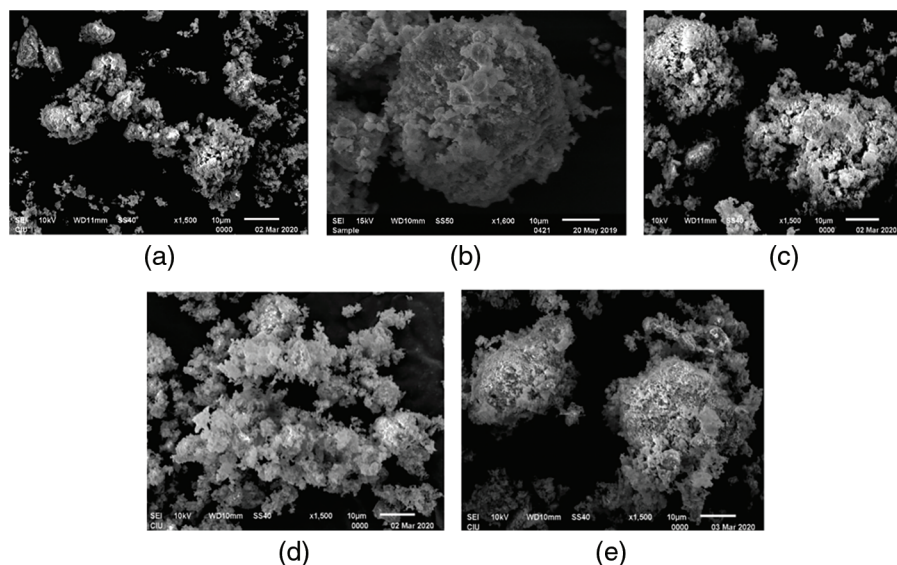


**Figure 12:** Morphology of Adobe sample before and after calcination at  $750^\circ\text{C}$  for different durations. (a) Raw AB, (b) 750 AB (1 h), (c) 750 AB (3 h), (d) 750 AB (5 h), (e) 750 AB (7 h)

#### 4.6 Slump and Flowability of Fresh Alkali-Activated Waste Stabilized Adobe-Slag Pastes

Incorporation of GGBFS in different percentages in the alkali-activated high-volume optimum calcined waste-stabilized Adobe pastes caused an increase in the slump value for all mixes as shown in Fig. 13. GGBFS with 5%, 10%, 15%, 20%, 25%, and 30% as partial replacement of optimum calcined waste-stabilized Adobe in the mixes show a difference in slump values. The slight reduction in the slump value

of the mix (100AB) in comparison with the mix (100ABW) is because of the sticky nature of the alkaline activator.

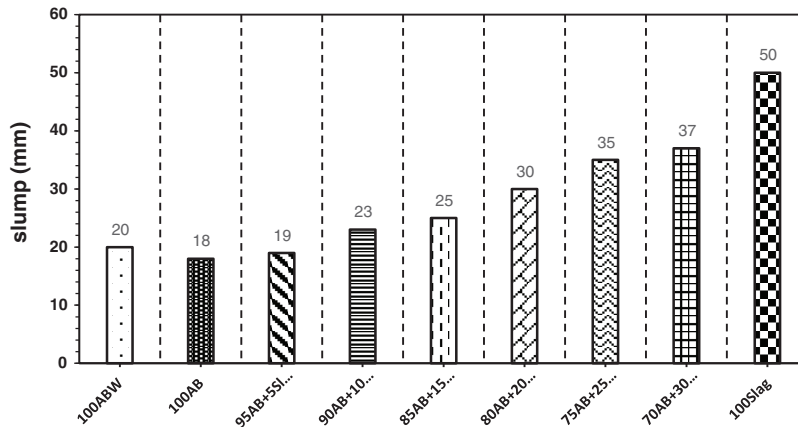


**Figure 13:** Mini slump values for fresh paste samples

The flow values of fresh alkali-activated high-volume optimum calcined waste stabilized Adobe-Slag pastes with varying GGBFS contents are present in Fig. 14. The flow value of the mix (100AB) was minimum, which was (110 mm). The sticky nature of the alkaline activator used in the preparation of mix (100AB) in comparison with water used in the mix (100ABW) caused a slight reduction in the flow value. The flow value of the mix (100AB) is 58.82% of the flow value of the control mix (100Slag). When 5% of GGBFS was added, the flow value of fresh paste increased slightly to 119 mm, which is 63.63% of the flow value of the control mix. With the increase of GGBFS content to 10%, 15%, 20%, 25% and 30%, the flow value of the fresh pastes were 76.47%, 76.47%, 79.14%, 80.74% and 82.89% of the flow value of control mix, respectively. The Incorporation of GGBFS in the mixes caused an increase in the flowability, which may be a result of the smaller surface area of slag 3092 cm<sup>2</sup>/g compared to the surface area 5618 cm<sup>2</sup>/g of optimum calcined waste-stabilized Adobe.

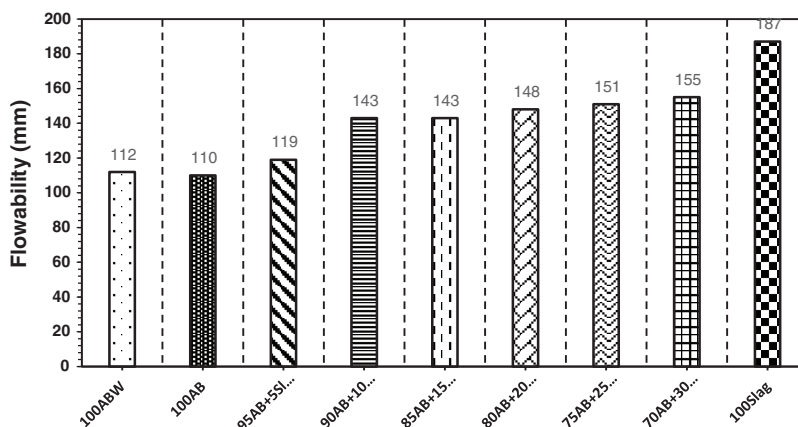


**Figure 14:** Flowability values for fresh paste samples

#### 4.7 Compressive Strength

The compressive strength of high-volume optimum calcined waste-stabilized Adobe-slag pastes was determined following the standard procedure prescribed in ASTM C109. The compressive strength is obtained by the average means of three identical specimens. The compressive strength for all mixes in this study at 3, 7, 14, and 28 days are shown in Table 1.

The compressive strength at different ages 3, 7, 14, and 28 days for the mix (100AB) is higher than the compressive strength of mix (100ABW), which consists of optimum calcined AB and water without alkaline activator. Based on this result, the calcination process is not enough to obtain a binder having a high compressive strength during early ages of curing at room temperature, without using an alkaline activator. Therefore, the activation process is necessary with calcination for this waste material.

All the prepared mixes were compared with alkali-activated GGBFS as a control mix. Incorporation of external sources of Ca like GGBFS can improve the strength at different ambient curing ages. The improvement in strength may be a result of forming more gel that comes from the activation of both waste- Adobe and GGBFS. Incorporation of GGBFS in alkali-activated optimum calcined AB by 0%, 5%, 10%, 15%, 20% and 25% till it reaches 30%, causing a sharp increase in the early age 3 days strength. Replacement of 30% of waste-stabilized Adobe by GGBFS gave a strength which is 60.70% of the strength of (100slag) at 3 days of room temperature curing.

There is a steady increase in the seventh-day strength of alkali-activated optimum calcined AB with different proportions 0%, 5%, 10%, 15%, 20%, 25%, and 30% of GGBFS in comparison with early age strength. The seventh-day strength of mixes (80AB + 20Slag), (75AB + 25Slag) and (70AB + 30Slag) is (40.59, 47.12 and 53.13) of the seventh-day strength of (100Slag) at room temperature. It can be said that the optimum alkali-activated waste stabilized Adobe-slag paste is (70AB + 30Slag) after 7 days of curing at room temperature. The early age strength in the aforementioned mixes may be controlled by the formation of the (N-A-S-H) framework due to the higher dissolution rate of aluminosilicate compound from waste-stabilized Adobe as the main precursor, where the use of two alkaline activators for the process of activation increases the alkalinity of the medium leading to a higher amount of soluble aluminates and silicate [45]. This assumption is comparable to a study done by [46,47], the strength development during the early age of alkali activation of a precursor rich in calcium is controlled by the formation of (N-A-S-H) framework. Part of the early age strength is attributed to the formation of C-S-H, but in a lesser amount [27,48,49].

Upon 14 days of ambient curing, it is observed that the optimum compressive strength was exhibited by mix (70AB + 30Slag) and it is 68.12% of the strength of the control mix. There is improvement in the strength with age (at 28-days of curing) for all mixes. The 28-day strength of the mix (70AB + 30Slag) is 71.37% of the control mix.

#### 5 Conclusion

The result of this research enables us to observe and understand the influence of calcination temperature and calcination duration on the chemical and mineralogical characteristics of the waste stabilized Adobe sample and to evaluate the possibility of using it as a new alkali-activated binder cured at room temperature.

1. Based on XRF analysis, increasing the calcination temperatures from (450°C–950°C) for the same calcination duration leads to an increase in the entire oxide content of the waste stabilized Adobe. The increase in the entire oxide content is noticeable up to 750°C, further increase in calcination temperature shows a slight or negligible increase in the chemical oxides
2. Prolonging the calcination duration for the same calcination temperature results in small or inconsiderable increases in the entire chemical oxide for the waste stabilized Adobe.

3. The calcination temperature for complete dehydroxylation of waste stabilized Adobe is 750°C, determined by TGA/DTA technique.
4. According to the XRD technique, calcination of the waste stabilized Adobe at 750°C for 1 h gave the lowest percentage of crystallinity as compared with other calcination durations. An extended duration beyond 1 h for 750°C calcination may lead to crystallization.
5. Prolonging the calcination duration for the same calcination temperature of 750°C affected the morphology of waste stabilized Adobe particles detected by SEM technique.
6. In all mixes and at all ambient curing ages, when slag content increases in the mix, the early age and later age strength of alkali-activated optimum calcined waste stabilized Adobe increase.
7. In this research, the optimum calcination condition to convert locally available waste-stabilized Adobe (AB) into a relatively unusual aluminosilicate precursor rich in calcium was achieved. Results show that the prepared alkali-activated binder obtained from this precursor alone does not seem to be suitable for adhesive application where high yield stress is needed or in applications requiring fast flows. On the other hand, it could gain ground when used as the main replacement of ground granulated blast furnace slag (GGBFS) to obtain an alkali-activated binder with satisfactory adhesive and rheological properties as an alternative to slag cement.
8. Calcined waste stabilized Adobe at 750°C for 1 h, as a new precursor for alkali-activated binder, shows the most promising performance considering environmental and economic aspects related to energy consumption. This new precursor not only extends the source of new materials for the solid-based alkali-activated binder but also solves the problem of space occupied by waste and pollution to yield better environmental outcomes.

**Funding Statement:** The authors received no specific funding for this study.

**Conflicts of Interest:** The authors declare that they have no conflicts of interest to report regarding the present study.

## References

1. Ojo, E. B., Mustapha, K., Teixeira, R. S., Savastano Jr, H. (2019). Development of unfired earthen building materials using muscovite-rich soils and alkali activators. *Case Studies in Construction Materials*, 11, e00262. DOI 10.1016/j.cscm.2019.e00262.
2. van Deventer, J. S., Provis, J. L., Duxson, P., Brice, D. G. (2010). Chemical research and climate change as drivers in the commercial adoption of alkali-activated materials. *Waste and Biomass Valorization*, 1(1), 145–155. DOI 10.1007/s12649-010-9015-9.
3. Pacheco-Torgal, F., Labrincha, J., Leonelli, C., Palomo, A., Chindaprasit, P. (2014). Prediction of the compressive strength of alkali-activated geopolymeric concrete binder by neuro-fuzzy modelling: A case study. *Handbook of Alkali Activated Cement, Mortars, and Concretes*, Amsterdam, Netherlands: Elsevier.
4. Pacheco-Torgal, F., Castro-Gomes, J., Jalali, S. (2008). Alkali-activated binders: A review: Part 1. Historical background, terminology, reaction mechanisms, and hydration products. *Construction and Building Materials*, 22(7), 1305–1314. DOI 10.1016/j.conbuildmat.2007.10.015.
5. Fernández-Jiménez, A., de la Torre, A. G., Palomo, A., López-Olmo, G., Alonso, M. M. et al. (2006). Quantitative determination of phases in the alkaline activation of fly ash. Part II: Degree of reaction. *Fuel*, 85(14–15), 1960–1969. DOI 10.1016/j.fuel.2006.04.006.
6. van Jaarsveld, J. G. S., van Deventer, J. S., Lukey, G. C. (2002). The effect of composition and temperature on the properties of fly ash-and kaolinite-based geopolymers. *Chemical Engineering Journal*, 89(1–3), 63–73. DOI 10.1016/S1385-8947(02)00025-6.

7. Zhang, L. (2013). Production of bricks from waste materials—A review. *Construction and Building Materials*, 47, 643–655. DOI 10.1016/j.conbuildmat.2013.05.043.
8. Diop, M. B., Grutzeck, M. W. (2008). The low-temperature process to create a brick. *Construction and Building Materials*, 22(6), 1114–1121. DOI 10.1016/j.conbuildmat.2007.03.004.
9. MacKenzie, K. J. (2009). Utilization of non-thermally activated clays in the production of geopolymers. In: *Geopolymers*, pp. 294–314. Sawston, UK: Woodhead Publishing.
10. Fernandez, R., Martirena, F., Scrivener, K. L. (2011). The origin of the pozzolanic activity of calcined clay minerals: A comparison between kaolinite, illite and montmorillonite. *Cement and Concrete Research*, 41(1), 113–122. DOI 10.1016/j.cemconres.2010.09.013.
11. Garg, N., Skibsted, J. (2014). Thermal activation of pure montmorillonite clay and its reactivity in cementitious systems. *The Journal of Physical Chemistry C*, 118(21), 11464–11477. DOI 10.1021/jp502529d.
12. Hollanders, S., Adriaens, R., Skibsted, J., Cizer, Ö., Elsen, J. (2016). Pozzolanic reactivity of pure calcined clays. *Applied Clay Science*, 132, 552–560. DOI 10.1016/j.clay.2016.08.003.
13. Tironi, A., Trezza, M. A., Scian, A. N., Irassar, E. F. (2014). Thermal analysis to assess the pozzolanic activity of calcined kaolinitic clays. *Journal of Thermal Analysis and Calorimetry*, 117(2), 547–556. DOI 10.1007/s10973-014-3816-1.
14. Liew, Y. M., Heah, C. Y., Kamarudin, H. (2016). Structure and properties of clay-based geopolymer cement: A review. *Progress in Materials Science*, 83, 595–629. DOI 10.1016/j.pmatsci.2016.08.002.
15. Luo, F. J., He, L., Pan, Z., Duan, W. H., Zhao, X. L. et al. (2013). Effect of very fine particles on workability and strength of concrete made with dune sand. *Construction and Building Materials*, 47, 131–137. DOI 10.1016/j.conbuildmat.2013.05.005.
16. Steen, C. (1971). An archaeologist's summary of adobe. *El Palacio*, 77(4), 29–38.
17. Isik, B., Tulbentci, T. (2008). Sustainable housing in island conditions using alker-gypsum-stabilized earth: A case study from northern Cyprus. *Building and Environment*, 43(9), 1426–1432. DOI 10.1016/j.buildenv.2007.06.002.
18. Brown, P. W., Clifton, J. R. (1978). Adobe I: The properties of adobe. *Studies in Conservation*, 23(4), 139–146.
19. Rodríguez, M. A., Saroza, B. (2006). Determination of the optimum composition of adobe brick for a school in Cuba. *Materiales de Construcción*, 56(282), 53–62.
20. Suwan, T., Fan, M. (2014). Influence of OPC replacement and manufacturing procedures on the properties of self-cured geopolymer. *Construction and Building Materials*, 73, 551–561. DOI 10.1016/j.conbuildmat.2014.09.065.
21. Nath, P., Sarker, P. K. (2015). Use of OPC to improve the setting and early strength properties of low calcium fly ash geopolymer concrete cured at room temperature. *Cement and Concrete Composites*, 55, 205–214. DOI 10.1016/j.cemconcomp.2014.08.008.
22. Deb, P. S., Nath, P., Sarker, P. K. (2014). The effects of ground granulated blast-furnace slag blending with fly ash and activator content on the workability and strength properties of geopolymer concrete cured at ambient temperature. *Materials & Design (1980–2015)*, 62, 32–39. DOI 10.1016/j.matdes.2014.05.001.
23. Kamseu, E., Djangang, C., Veronesi, P., Fernanda, A., Melo, U. C. et al. (2015). Transformation of the geopolymer gels to crystalline bonds in cold-setting refractory concretes pore evolution, mechanical strength, and microstructure. *Materials & Design*, 88, 336–344. DOI 10.1016/j.matdes.2015.08.151.
24. Kumar, S., Kumar, R., Mehrotra, S. P. (2010). Influence of granulated blast furnace slag on the reaction, structure, and properties of fly-ash based geopolymer. *Journal of Materials Science*, 45(3), 607–615. DOI 10.1007/s10853-009-3934-5.
25. Nuaklong, P., Sata, V., Chindapasirt, P. (2016). Influence of recycled aggregate on fly ash geopolymer concrete properties. *Journal of Cleaner Production*, 112, 2300–2307. DOI 10.1016/j.jclepro.2015.10.109.
26. Puligilla, S., Mondal, P. (2013). Role of slag in microstructural development and hardening of fly ash-slag geopolymer. *Cement and Concrete Research*, 43, 70–80. DOI 10.1016/j.cemconres.2012.10.004.
27. Xu, H., Gong, W., Syltebo, L., Izzo, K., Lutze, W. et al. (2014). Effect of blast furnace slag grades on fly-ash based geopolymer waste forms. *Fuel*, 133, 332–340. DOI 10.1016/j.fuel.2014.05.018.
28. ASTM C204-11 (2018). Standard Test Methods for Fineness of Hydraulic Cement by Air-Permeability Apparatus, ASTM International, West Conshohocken, PA, 2011. [www.astm.org](http://www.astm.org).

29. ASTM WK63516 (2018). New test method for measurement of fresh hydraulic cement paste spread using a mini-slump cone, ASTM International, West Conshohocken, PA, 2018. [www.astm.org](http://www.astm.org).
30. Cravero, F., Fernández, L., Marfil, S., Sánchez, M., Maiza, P. et al. (2016). Spheroidal halloysites from patagonia, Argentina: Some aspects of their formation and applications. *Applied Clay Science*, 131, 48–58. DOI 10.1016/j.clay.2016.01.011.
31. Todor, D. N. (1976). *Thermal analysis of minerals*. Abacus Press. <https://www.sciencedirect.com/science/article/pii/B9780123999023500245>.
32. Jemaï, M. B. M. B., Sdiri, A., Errais, E., Duplay, J., Saleh, I. B. et al. (2015). Characterization of the Ain khemouda halloysite (Western Tunisia) for ceramic industry. *Journal of African Earth Sciences*, 111, 194–201. DOI 10.1016/j.jafrearsci.2015.07.014.
33. Bratov, B., Doykov, I., Ninov, J., Lenchev, A. (2018). Pozzolanic activity assessment of calcined clays with complex minerals content. *Advances in Cement Research*, 30(3), 103–112. DOI 10.1680/jadcr.17.00057.
34. Kadir, S., Külah, T., Eren, M., Önalgil, N., Gürel, A. (2014). Mineralogical and geochemical characteristics and genesis of the güzelyurt alunite-bearing kaolinite deposit within the late miocene gördeles ignimbrite, central anatolia, Turkey. *Clays and Clay Minerals*, 62(6), 477–499. DOI 10.1346/CCMN.2014.0620603.
35. Majedová, J. (2003). FTIR techniques in clay mineral studies—Review. *Vibrational Spectroscopy*, 31, 1–10. DOI 10.1016/S0924-2031(02)00065-6.
36. Sumner, M. E. (1999). *Handbook of soil science*. Florida, USA: CRC Press.
37. Ratcliffe, C. I., Irish, D. E. (1982). Vibrational spectral studies of solutions at elevated temperatures and pressures. 5. Raman studies of liquid water up to 300. degree. *C. Journal of Physical Chemistry*, 86(25), 4897–4905. DOI 10.1021/j100222a013.
38. Park, J. H., Min, D. J., Song, H. S. (2002). Structural investigation of CaO-Al<sub>2</sub>O<sub>3</sub> and CaO-Al<sub>2</sub>O<sub>3</sub>-CaF<sub>2</sub> slags via Fourier transform infrared spectra. *ISIJ International*, 42(1), 38–43. DOI 10.2355/isijinternational.42.38.
39. Böttcher, M. E., Gehlken, P. L., Steele, D. F. (1997). Characterization of inorganic and biogenic magnesian calcites by Fourier transform infrared spectroscopy. *Solid State Ionics*, 101, 1379–1385. DOI 10.1016/S0167-2738(97)00235-X.
40. Parthasarathy, G., Sharma, S. D., Srinivasan, R., Krishnamurthy, P. (2001). Mineralogical and geochemical study on carbonate veins of the salem-attur fault zone, southern India: Evidence for carbonatitic affinity. *Journal of Geological Society of India*, 58(1), 15–26.
41. Criado, M., Fernández-Jiménez, A., Palomo, A. (2007). Alkali activation of fly ash: Effect of the SiO<sub>2</sub>/Na<sub>2</sub>O ratio: Part I: FTIR study. *Microporous and Mesoporous Materials*, 106(1–3), 180–191. DOI 10.1016/j.micromeso.2007.02.055.
42. Chakchouk, A., Samet, B., Mnif, T. (2006). Study on the potential use of Tunisian clays as pozzolanic material. *Applied Clay Science*, 33(2), 79–88. DOI 10.1016/j.clay.2006.03.009.
43. Duxson, P., Provis, J. L., Lukey, G. C., Mallicoat, S. W., Kriven, W. M. et al. (2005). Understanding the relationship between geopolymer composition, microstructure, and mechanical properties. *Colloids and Surfaces A: Physicochemical and Engineering Aspects*, 269(1–3), 47–58. DOI 10.1016/j.colsurfa.2005.06.060.
44. Hanjitsuwan, S., Hunpratub, S., Thongbai, P., Maensiri, S., Sata, V. et al. (2014). Effects of NaOH concentrations on physical and electrical properties of high calcium fly ash geopolymer paste. *Cement and Concrete Composites*, 45, 9–14. DOI 10.1016/j.cemconcomp.2013.09.012.
45. García-Lodeiro, I., Fernández-Jiménez, A., Palomo, A., Macphee, D. E. (2010). Effect of calcium additions on N-A-S-H cementitious gels. *Journal of the American Ceramic Society*, 93(7), 1934–1940. DOI 10.1111/j.1551-2916.2010.03668.x.
46. Richardson, I. G., Brough, A. R., Groves, G. W., Dobson, C. M. (1994). The characterization of hardened alkali-activated blast-furnace slag pastes and the nature of the calcium silicate hydrate (CSH) phase. *Cement and Concrete Research*, 24(5), 813–829. DOI 10.1016/0008-8846(94)90002-7.
47. Saha, S., Rajasekaran, C. (2017). Enhancement of the properties of fly-ash based geopolymer paste by incorporating ground granulated blast furnace slag. *Construction and Building Materials*, 146, 615–620. DOI 10.1016/j.conbuildmat.2017.04.139.